Supplementary materials for

Interpretable Machine Learning Quantifies Composition and Size Controls on Aerosol Spectral Absorption

Wenfang Wang[1], Pengfei Tian[1,2*], Shuhua Zeng[1], Yifei Zhang[1], Zeren Yu[1], Chen Cui[1], Yunfei Wu[3], Min Chen[1], Lei Zhang[1,2]

[1] Key Laboratory for Semi-Arid Climate Change of the Ministry of Education, College of Atmospheric Sciences, Lanzhou University, Lanzhou 730000, China.

[2] Collaborative Innovation Center for Western Ecological Safety, Lanzhou University, Lanzhou 730000, China.

[3] State Key Laboratory of Atmospheric Environment and Extreme Meteorology, Institute of Atmospheric Physics, Chinese Academy of Sciences, Beijing 100029, China.

Corresponding author: P. Tian (tianpf@lzu.edu.cn) and M. Chen (chenmin@lzu.edu.cn)

Contents of this file

Text S1. Stokes Diameter Conversion Aerodynamic Diameter.

SMPS used 8.82-310.6 nm data and APS used 0.523-19.81 μm data. For particle density of 1.7 g·cm^{-3} the particle diameter 310.6 nm corresponds to the aerodynamic diameter $D_a = \sqrt{\rho_p/\rho_0}\, D_p \cong 405\, nm$, where ρ_0 = 1 g·cm^{-3}, and ρ =1.7 g·cm^{-3} is constant over the whole size range (Shang et al., 2018).

Text S2. Offline chemical analysis of filter samples.

For WSII, one quarter of each filter was cut into small pieces and extracted with 10 mL ultrapure water (>18 MΩ·cm) by ultrasonication for 30 min; the extraction was repeated once, and the combined extracts were brought to 25 mL with ultrapure water. The extract was filtered through a 0.45 μm membrane (GHP, model 4563, Pall Inc., USA) and stored at 4 °C prior to ion chromatography (881 Compact IC Pro, Metrohm, Switzerland; and ICS-1500, Dionex Inc., USA). Cations (Na^+, K^+, NH_4^+, Ca^{2+}, Mg^{2+}) were measured with ion chromatograph (881 Compact IC Pro, Metrohm, Switzerland) equipped with a Metrosep C4 column. The eluent was 1.75 mM HNO_3 + 0.75 mM dipicolinic acid. Anions (Cl^-, NO_3^-, SO_4^{2-}) were measured with an ion chromatograph (ICS-1500, Dionex Inc., USA) equipped with an IonPac AS22 column. The eluent was 4.5 mM Na_2CO_3 + 1.4 mM $NaHCO_3$. The method detection limits (MDLs) were 0.05, 0.10, 0.19, 0.04, 0.01, 0.02, and 0.02mg·L^{-1} for K^+, NH_4^+, Ca^{2+}, Mg^{2+}, Cl^-, NO_3^-, and SO_4^{2-}, respectively. Due to generally elevated Na^+ blanks associated with quartz-fiber filters and glassware, Na^+ was excluded here.

One quarter of each quartz-fiber filter was used for elemental analysis. The filter

41 portion was cut into small pieces and transferred to a digestion bottle. Concentrated
42 nitric acid (HNO_3, 68%, 10 mL) was added, and the mixture was heated until digestion
43 was complete. After cooling, the digest was diluted to 20 mL with ultrapure water. The
44 resulting solutions were analyzed for Al, Ca, Mg, Fe, and Ti using inductively coupled
45 plasma–atomic emission spectrometry (ICP-AES; iCAP 7400, Thermo, USA). The
46 MDLs were 0.02, 0.19, 0.02, 0.07, and 0.00 $mg \cdot L^{-1}$ for Al, Ca, Mg, Fe, and Ti,
47 respectively.

48 A circular area of each filter sample using a 0.504 cm^2 punch was cut for the
49 analysis of OC and EC by thermal/optical carbon analyzer (DRI Model 2015, USA)
50 following the thermal/optical reflectance (TOR) method (Chow et al., 2007). Briefly, a
51 filter punch was progressively heated to evolve carbon fractions under stepwise
52 temperature programs. OC fractions were evolved in a pure He atmosphere at 120 °C
53 (OC1), 250 °C (OC2), 450 °C (OC3), and 550 °C (OC4). Subsequently, EC fractions
54 were evolved in an oxidizing atmosphere of 2% O_2 and 98% He at 550 °C (EC1),
55 700 °C (EC2), and 800 °C (EC3). Evolved carbon was oxidized to CO_2 and then
56 reduced to CH_4 for detection using a flame ionization detector. Pyrolyzed organic
57 carbon (OPC) was monitored using the laser reflectance signal and was defined when
58 the reflected laser signal returned to its initial value after the introduction of O_2 into the
59 analysis atmosphere. OC was calculated as OC1 + OC2 + OC3 + OC4 + OPC, whereas
60 EC was calculated as EC1 + EC2 + EC3 − OPC. The MDLs were 0.18 and 0.04 $\mu g \cdot m^{-2}$
61 for OC and EC, respectively.

Table S1. Correlation Matrix of Aerosol Chemical Species

	NH_4^+	K^+	Mg^{2+}	Ca^{2+}	Cl^-	SO_4^{2-}	NO_3^-	OC	EC	Al	Ca	Fe	Mg	Ti
NH_4^+	1.00	0.90	0.25	-0.07	0.50	0.95	0.99	0.83	0.78	0.08	0.07	0.34	0.23	0.20
K^+		1.00	0.36	-0.07	0.52	0.85	0.89	0.84	0.82	0.03	-0.03	0.24	0.20	0.09
Mg^{2+}			1.00	0.76	0.74	0.24	0.23	0.35	0.33	0.30	0.31	0.03	0.34	0.08
Ca^{2+}				1.00	0.33	-0.05	-0.07	-0.06	-0.05	0.11	0.11	-0.15	0.11	-0.09
Cl^-					1.00	0.45	0.48	0.57	0.54	0.35	0.39	0.13	0.40	0.18
SO_4^{2-}						1.00	0.95	0.76	0.72	0.09	0.08	0.27	0.19	0.21
NO_3^-							1.00	0.82	0.77	0.07	0.06	0.34	0.23	0.19
OC								1.00	0.82	0.10	0.10	0.35	0.22	0.08
EC									1.00	0.00	-0.02	0.14	0.12	0.00
Al										1.00	0.88	0.07	0.91	0.11
Ca											1.00	0.15	0.86	0.20
Fe												1.00	0.11	0.60
Mg													1.00	0.07
Ti														1.00

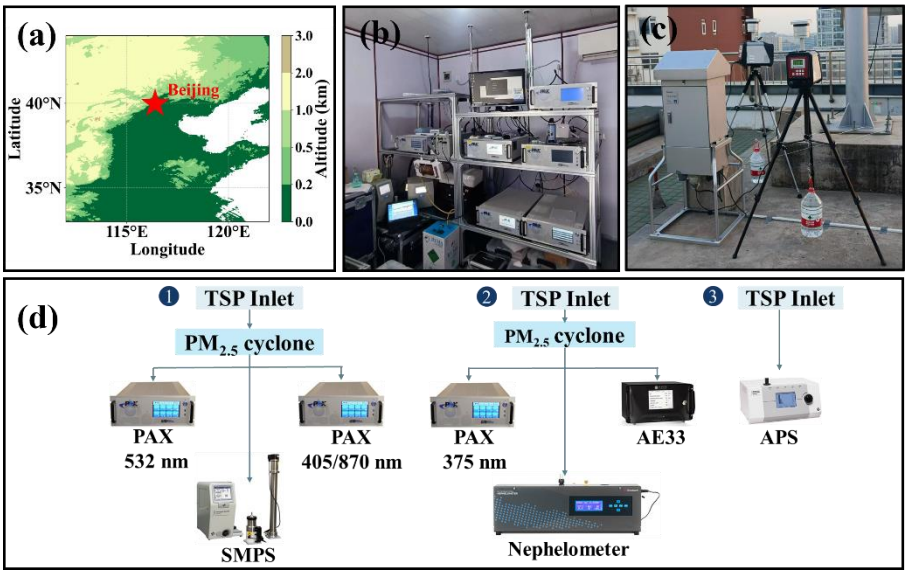

Figure S1. Geographic location of observation site and observation instruments. (a) Geographical map, location of the field campaign. (b, c) Photographs during the field campaign. (d) Airflow settings of the online instruments.

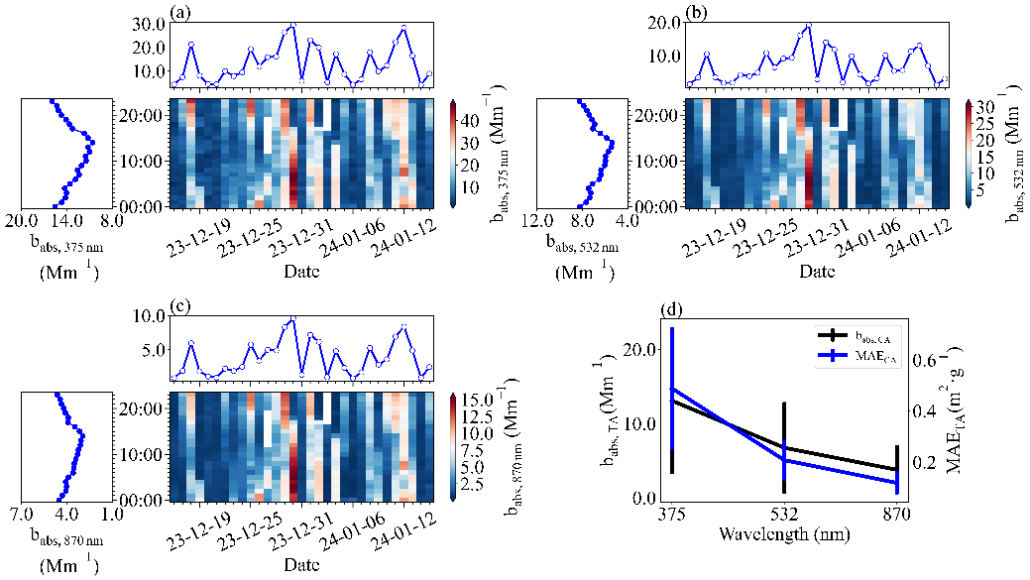

Figure S2. (a, b, c) The time series of mass concentrations of absorption coefficients at 375, 405, 870 nm, mass absorption efficiency at 375, 405, 870 nm. (d). Wavelength dependence of absorption coefficients and mass absorption efficiency.

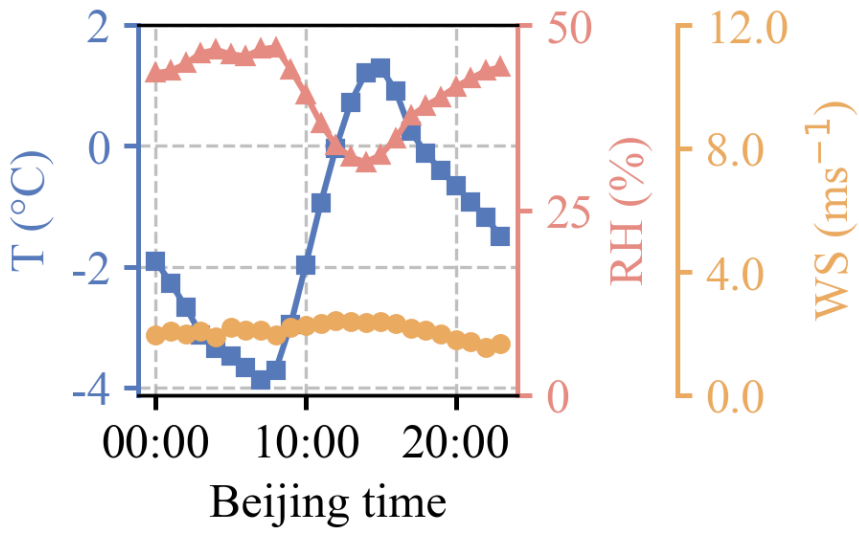

Figure S3. Daily variation of Temperature, Relative Humidity, Wind Speed.

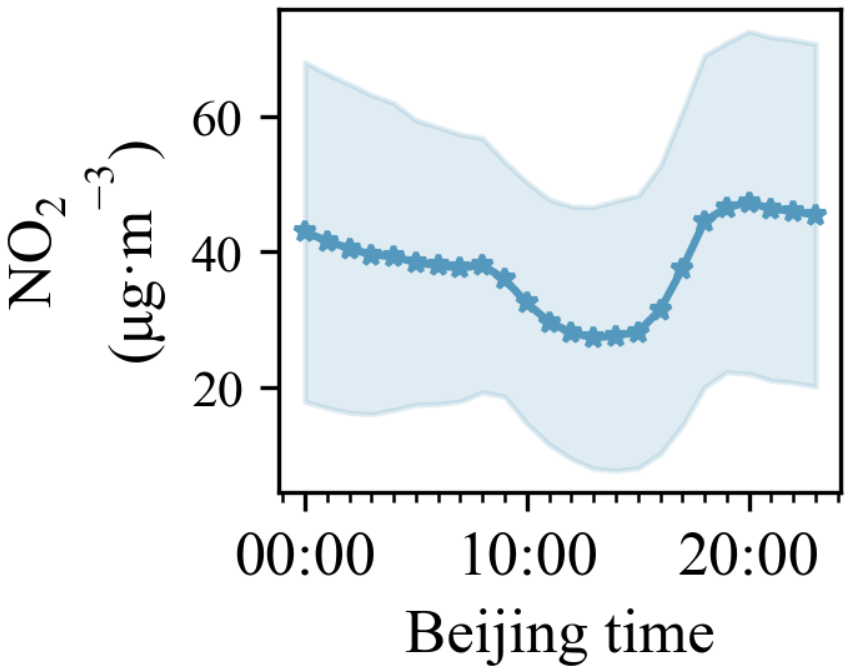

74

75 **Figure S4.** Daily variation of nitrogen dioxide (NO_2). Hourly NO_2 mass concentrations were
76 obtained from the China National Environmental Monitoring Network for the Beijing urban
77 site.

78

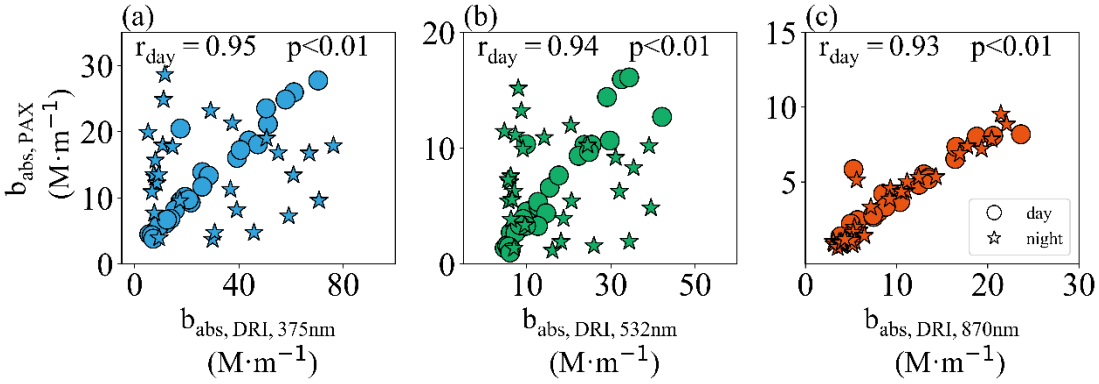

79

80 **Figure S5.** Scatter plots of the aerosol absorption coefficients between PAX and DRI. (a) 375
81 nm. (b) 532 nm. (c) 870nm.

82

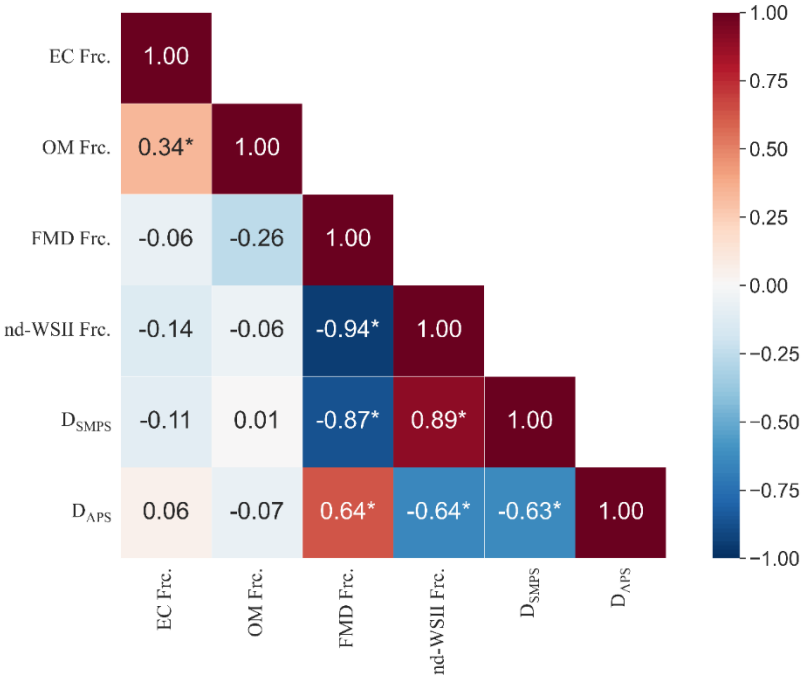

Figure S6. Correlation analysis among chemical composition (non-dust water-soluble ions (nd-WSII), fine mineral dust (FMD), elemental carbon (EC), organic matter (OM)) fraction and size parameter (fine-mode mean diameter from SMPS (D_{SMPS}), coarse-mode mean diameter from APS (D_{APS}).

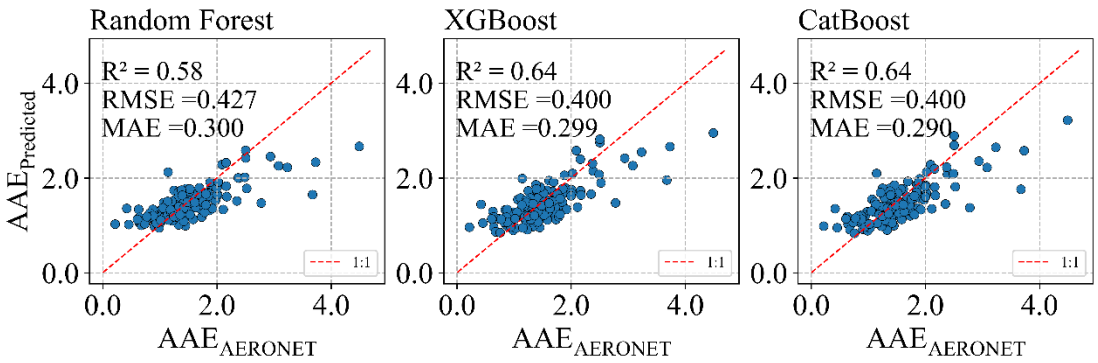

Figure S7. Comparison of aerosol absorption Ångström exponent (AAE) predictions and AERONET observations by different models.

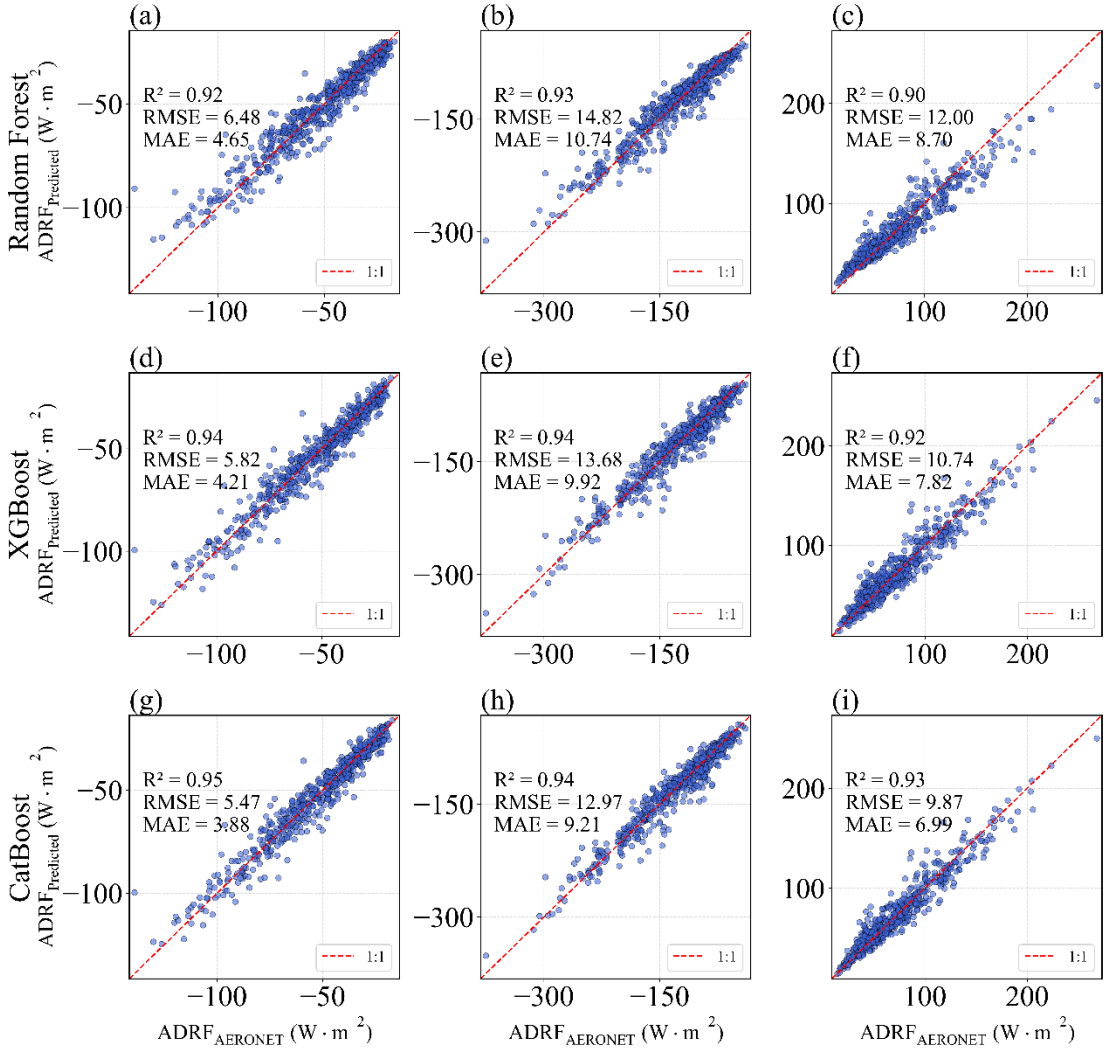

92

93 **Figure S8.** Comparison of aerosol direct radiative forcing (ADRF) predictions and AERONET

94 observations by different models.

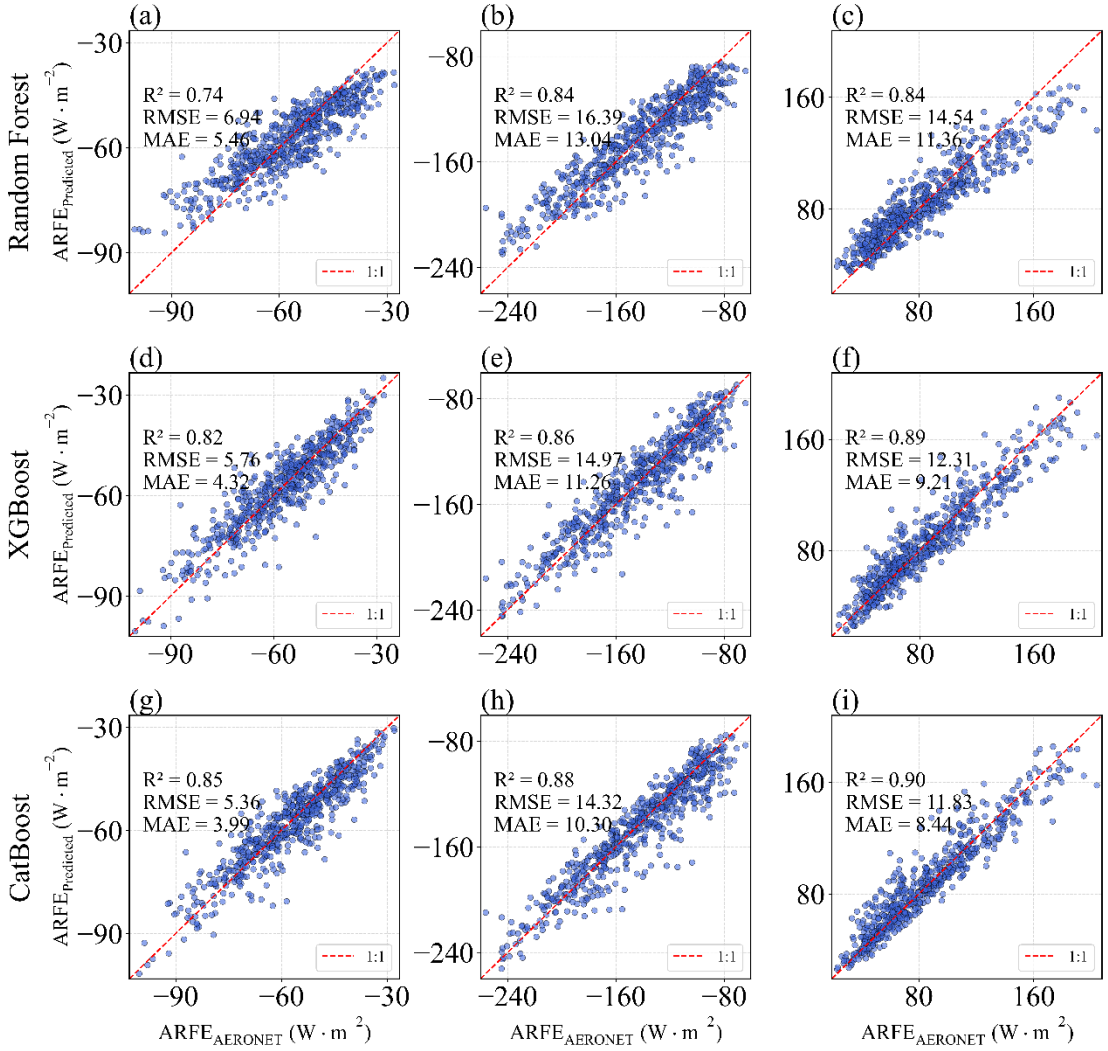

Figure S9. Comparison of aerosol radiative forcing efficiency (ARFE) predictions and AERONET observations by different models.

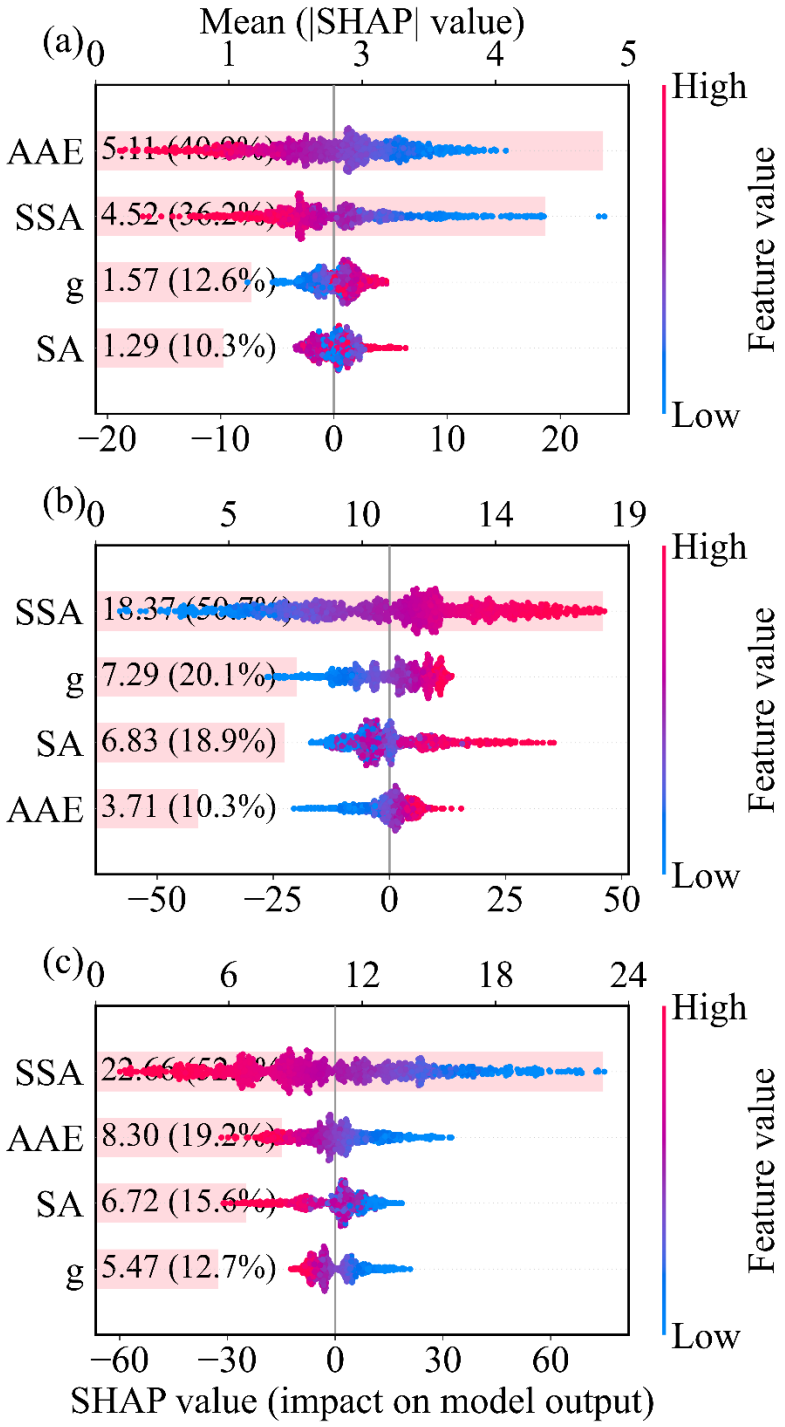

Figure S10. SHAP analysis with AOD fixed at its 25th percentile quantifies the relative contributions of single scattering albedo (SSA), asymmetry parameter (g), surface albedo (SA) and columnar AAE in driving aerosol radiative forcing efficiency (ARFE) variations at the top of the atmosphere (a), bottom (b), and in the atmosphere (c). The mean absolute SHAP values

(numbers in parentheses) indicate the relative contribution of each predictor to the model output.

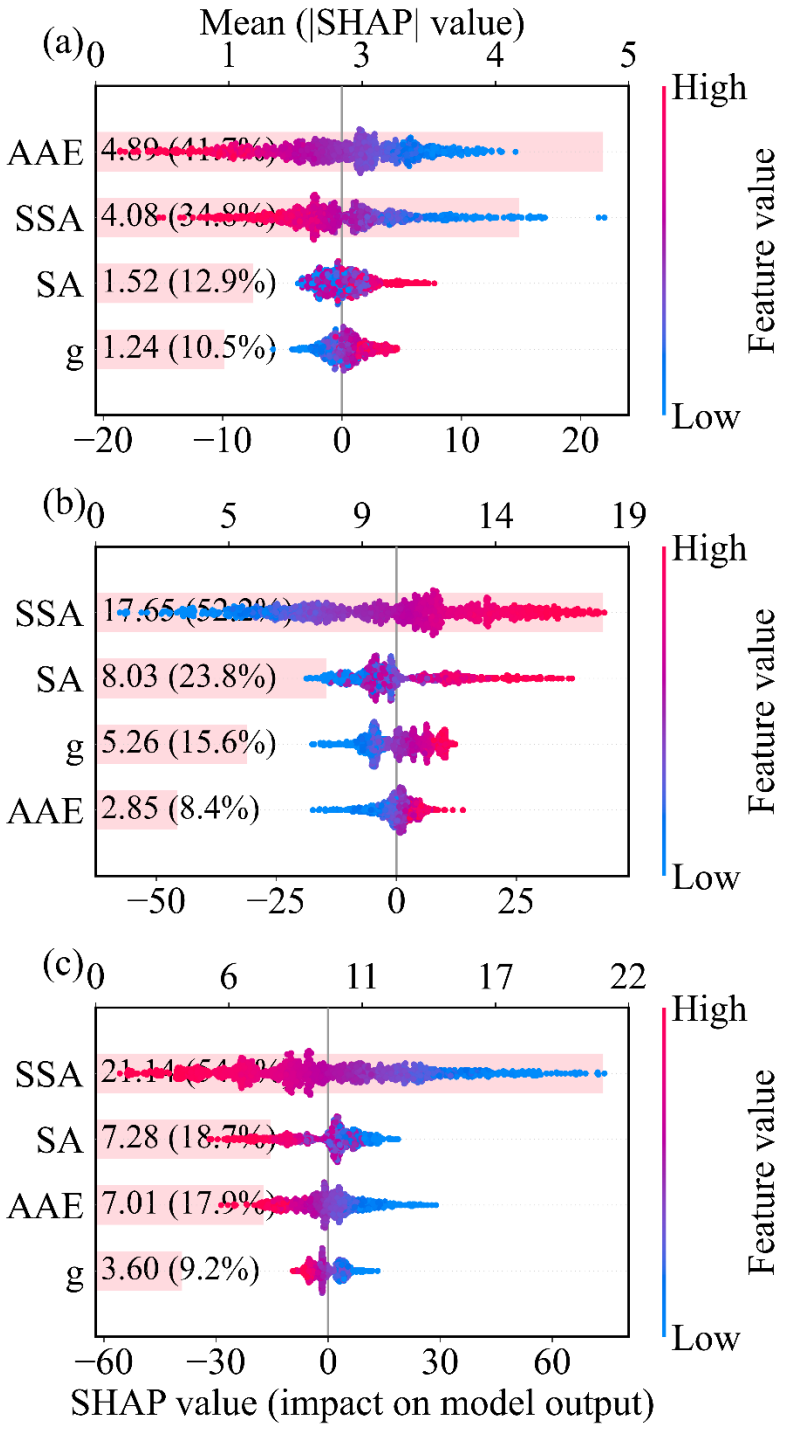

Figure S11. Same as Figure S10, except aerosol optical depth (AOD) is fixed at its 75th percentile.

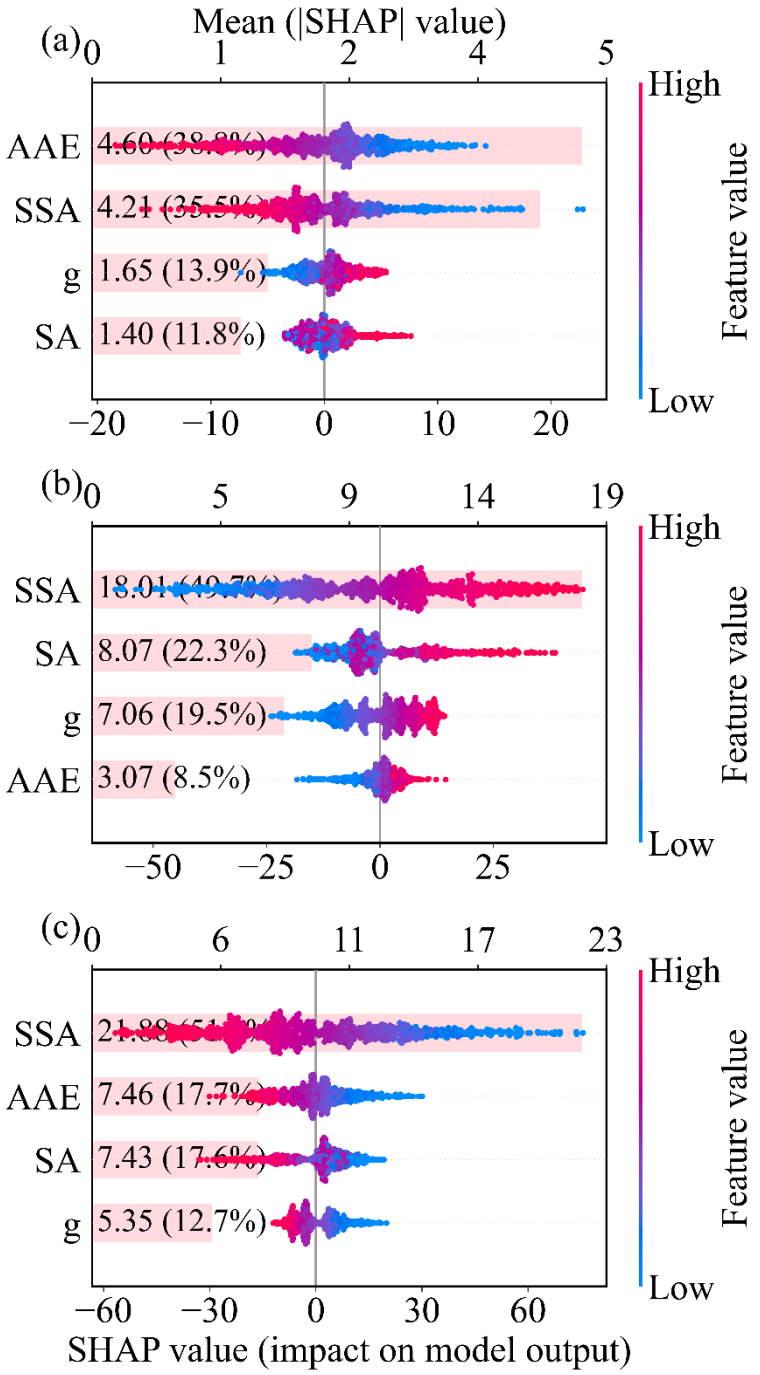

Figure S12. Same as Figure S10, except aerosol optical depth (AOD) is fixed at its mean value.

References

Shang, D., Hu, M., Zheng, J., Qin, Y., Du, Z., Li, M., Fang, J., Peng, J., Wu, Y., Lu, S., and Guo, S.: Particle number size distribution and new particle formation under the influence of biomass burning at a high altitude background site at Mt. Yulong (3410 m), China, Atmos. Chem. Phys., 18, 15687–15703, https://doi.org/10.5194/acp-18-15687-2018, 2018.

Chow, J. C., Watson, J. G., Chen, L.-W. A., Chang, M. C. O., Robinson, N. F., Trimble, D., and Kohl, S.: The IMPROVE_A Temperature Protocol for Thermal/Optical Carbon Analysis: Maintaining Consistency with a Long-Term Database, Journal of the Air & Waste Management Association, 57, 1014–1023, https://doi.org/10.3155/1047-3289.57.9.1014, 2007.